IEEE Access
Multidisciplinary ⋮ Rapid Review ⋮ Open Access Journal

Received December 12, 2019, accepted December 23, 2019, date of publication December 27, 2019,
date of current version January 9, 2020.

Digital Object Identifier 10.1109/ACCESS.2019.2962722

Robust Backstepping Sliding Mode Control for a Quadrotor Trajectory Tracking Application

DHAFER J. ALMAKHLES, (Member, IEEE)
Renewable Energy Laboratory, College of Engineering, Prince Sultan University, Riyadh 11586, Saudi Arabia
Communications and Networks Department, Prince Sultan University, Riyadh 11586, Saudi Arabia

e-mail: dalmakhles@psu.edu.sa

This work was supported by the Renewable Energy Laboratory, College of Engineering, Prince Sultan University.

ABSTRACT This paper proposes a robust position control scheme for a quadrotor UAV system under uncertainties. The proposed control algorithms combine integral sliding mode and backstepping sliding mode controllers in a double-loop control structure (i.e., inner-outer loop control). The design of the proposed controller is divided into two subcontrollers, namely, attitude and position controllers for the quadrotor. In this work, a nonsimplified six-degree-of-freedom quadrotor model is first established in the presence of disturbances. Afterward, we develop a robust backstepping sliding mode controller for the attitude control of the quadrotor. Next, a robust integral sliding mode controller is designed for the outer loop of the quadrotor to ensure the position trajectory tracking capability in the presence of disturbances. The stability and performance of the quadrotor is thoroughly investigated using Lyapunov stability analysis. Numerical simulations demonstrate the effectiveness of the developed solutions for a quadrotor.

INDEX TERMS Backstepping control, sliding mode control, robustness, disturbance, quadrotor, unmanned aerial vehicle (UAV), quadcopter.

I. INTRODUCTION

Unmanned aerial vehicles (UAVs) have a wide range of practical and innovative uses, ranging from military applications such as defense, exploration, military surveillance, navigation, and safety inspections to civil applications such as media, entertainment, journalism, agriculture, shipping, and delivery. Around the globe, the number of applications of quadrotor UAVs has been increasing over the last few years in particular thanks to their precise maneuverability, high robustness, and ability to fly in any directions, land and take off in limited space, and hover precisely above the desired target. Indeed, all these unique features make quadrotors particularly promising among currently emerging techniques [1]. However, certain factors related to safety, security and reliability limit what can be achieved with this technology. For example, a high degree of autonomy of quadrotors is an essential requirements for many quadrotor applications. Thus, designing an unmanned flight system, whether it functions autonomously or nonautonomously (remotely controlled from a ground station), often poses many engineering challenges, including challenges related to sensor technology and hardware and software designs. Because a quadrotor UAV is a very complex control system, such systems have received considerable attention from researchers in the field of automatic control.

The design of controllers for quadrotors faces at least two formidable challenges from the perspective of control theory. First, quadrotors are multiple-input multiple-output (MIMO) unstable nonlinear systems. Such a control system is coupled and under-actuated due to its six degrees of freedom (DOFs) and four actuators. Second, quadrotors, like other types of UAVs, are always subject to external and internal disturbances, model uncertainty, and parametric perturbations. To ensure the stability of quadrotors, robust controllers are often developed to reduce the effects of disturbances and uncertainties.

The development of effective control strategies for quadrotors has been extensively studied and applied in a diverse range of applications for quadrotor applications. For simplicity, quadrotors are initially linearized around preselected equilibrium conditions. The operation point(s) of quadrotors are usually chosen to be a hover point or any other tracking point. As a result, various linear control algorithms such as proportional-integral-derivative (PID) control [2]–[5], proportional-derivative (PD) control [6], proportional plus

The associate editor coordinating the review of this manuscript and approving it for publication was Sun Junwei.

This work is licensed under a Creative Commons Attribution 4.0 License. For more information, see http://creativecommons.org/licenses/by/4.0/

second-order differentiator (PD^2) control [7], and linear quadratic regulator/Gaussian (LQR/LQG) control [8], have been applied to achieve the control objectives. These traditional linear controllers for quadrotors, which involve linear approximations of the system dynamics around single or multiple operating points, are desirable in realistic autopilot design. However, these methods face the drawback of performance degradation when the aircraft deviates from its designed operating points. Strictly speaking, the inherent nonlinearity and strong coupling properties of a quadrotor pose many limitations for these linear control strategies.

To overcome the limitations of linear strategies, a variety of nonlinear algorithms have been proposed in the literature. Generally speaking, robust nonlinear techniques efficiently increase the stability of the basin of attraction and achieve acceptable performance under unpredictable changes in the environment, enabling aggressive maneuvering and accurate trajectory tracking. Nonlinear control techniques were initially considered in [9] and [10] to autonomously control the vertical take-off and landing (VTOL) of a 3-DOF helicopter and aircraft. The motion of a fixed-wing helicopter is controlled through the force produced by varying the angular speeds of two rotors: the main rotor and tail rotor. In contrast to a fixed-wing helicopter, a quadrotor has 6-DOF airframe dynamics and strong coupling of the yaw, pitch and roll motions, which render the control design much more challenging [11]. However, in some cases, the design of a controller for a classical helicopter could be applied to a quadrotor with some modifications and vice versa. Many studies have considered multiple nonlinear controllers for different autonomous control designs of quadrotors, such as feedback linearization [12]–[15], dynamic inversion [16], singular perturbation [17], sliding mode control [18]–[21], backstepping [18], [22]–[28], and other related adaptive nonlinear controllers [10], [18], [29], [30]. Considering fault tolerant control (FTC), various nonlinear algorithms including backstepping, sliding mode and adaptive FTC approaches for quadrotor attitude and altitude tracking can be found in [31], [32], and references therein.

In the context of nonlinear control, [13] was the first work to propose a nonlinear controller for a quadrotor, in which the authors designed a dynamic feedback controller based on so-called exact feedback linearization for the position tracking of the quadrotor. Simulation of their proposed control strategy showed acceptable performance even in the presence of external disturbances such as wind and turbulence. Nonetheless, designing a controller using only the feedback linearization approach requires an accurate model with stable zero dynamic in order to cancel out nonlinear terms (see [10], [33]). Thus, real-time implementation using a feedback linearization controller is unfeasible since the zero dynamics of a quadrotor are "marginally" stable, and it is difficult to achieve an accurate model in practice due to the unavoidable internal uncertainties such unmodeled dynamic uncertainties and parametric uncertainties [10], [15]. Although the authors of [13] utilized the simplified model of a quadrotor presented in [9], they found that controlled quadrotor was sensitive to sensor noise as well as modeling uncertainty. In this context, dynamic inversion, presented in [16] and falling under the definition of feedback linearization control to some sense, can achieve satisfactory trajectory tracking only if the residual or internal dynamics are stable. This situation renders the control design much more challenging in the presence of marginally stable zero dynamics. Thus, if such a feedback linearization approach is to be implemented in practice, then it should be accompanied by another control technique, such as neural networks or sliding mode control [14].

With recent dramatic developments in control strategies for quadrotors, increasing attention has been paid to recent robust control approaches such as sliding mode and backstepping control. Generally speaking, a controller designed for quadrotors is divided into two subcontrollers: an attitude controller (inner loop) and an altitude/position controller (outer loop). For example, in [19], the authors proposed a sliding mode altitude controller for a quadrotor in which they replaced the sign function with a saturation function to significantly reduce the effect of chattering. This work was extended in [20] by using integral sliding mode altitude control for a quadrotor. In [21], [34], the authors proposed an integral sliding mode controller for the attitude control of a quadrotor system and a PID and LQR controller for position control. A terminal sliding mode position controller and a conventional sliding mode attitude control were proposed in [35].

Some other researchers have also attempted the design of backstepping controllers for quadrotor systems. For example, [18], [24], [36] presented backstepping controllers for the position control of the quadrotors. Nonetheless, most authors have not considered uncertainties in their models and controller designs. In a recent work [37], a robust backstepping controller was successfully designed for the position control of a quadrotor considering a specific type of uncertainty, i.e., constant and maintained uncertainty. However, in many existing works in the literature, backstepping controllers have only been developed for the position (i.e., outer-loop) control of quadrotors [18], [38]. According to the literature, it is very important to focus more on the attitude control of a quadrotor even when position control cannot be achieved.

Using this as a motivation, our paper presents a new robust nonlinear control strategy for a quadrotor under uncertainties. The design of the proposed controller is divided into two subcontrollers: an attitude controller and a position controller. In this paper, we develop a robust backstepping sliding mode controller for the attitude control of the quadrotor and an integral sliding mode controller to ensure the position trajectory tracking capability of the quadrotor in the presence of external disturbances. The main contributions of this paper are summarized as follows:

1) A nonsimplified 6-DOF dynamic model of a quadrotor based on the Newton–Euler formula with additive estimated internal and external disturbances is established.
2) A robust nonlinear controller, namely, a backstepping sliding mode controller, is designed for the inner

control loop (i.e., attitude control) of the quadrotor in order to achieve hover stability.

3) A robust integral sliding mode controller is designed the outer control loop (i.e., position control) of the quadrotor to generate the desired Euler angles.
4) Based on the hierarchical control scheme, the designed controllers correspond to a rotational controller and a translational controller and their stability is validated by the Lyapunov stability theorem. More precisely, the proposed controllers can overcome the effect of disturbance.
5) The proposed theoretical results are validated by presenting the simulation results for the quadrotor model ender the influence of internal and external disturbances. The necessity of the developed robust controllers is clearly shown.

To the best of our knowledge, this is the first work in the literature that uses a robust backstepping sliding mode controller for the attitude control of a quadrotor and a robust integral sliding mode controller for the position control.

The rest of this paper is organized as follows. The 6-DOF dynamic model is developed in Section II. Afterward, the robust backstepping sliding mode controller for the attitude control of the quadrotor is designed in Section III.A., and the robust integral sliding mode controller is developed in Section III.B. Numerical simulations are presented to demonstrate the effectiveness of the developed solutions for a quadrotor in Section IV. Conclusions and future work are discussed in Section V.

II. QUADROTOR MODEL

The Newton-Euler equations of motion are commonly used to model quadrotors with respect to two observational frames of reference: the body-fixed frame and the inertial frame. The body-fixed frame, which is denoted by $\Sigma_{\mathcal{FB}}$, is attached to the center of mass of the quadrotor. Let $\Sigma_{\mathcal{FG}}$ represent the inertial frame, with $\boldsymbol{p} = [x, y, z]^T$ denoting the Euclidean position of the quadrotor w.r.t. $\Sigma_{\mathcal{FG}}$. The attitude of the quadrotor is denoted by $\boldsymbol{\eta} = [\phi, \theta, \psi]^T$, in which $|\phi| < \frac{\pi}{2}$, $|\theta| < \frac{\pi}{2}$, and $|\psi| < \pi$. The associated angular velocity is denoted by $\boldsymbol{\xi} = [p, q, r]^T$. The dynamic model of the quadrotor includes the linear translational velocity $\boldsymbol{\upsilon} = [\upsilon^x, \upsilon^y, \upsilon^z]^T$.

The rotation matrix from $\Sigma_{\mathcal{FB}}$ to $\Sigma_{\mathcal{FG}}$ is obtained as follows:

$$\boldsymbol{R}(\boldsymbol{\eta}) = \begin{bmatrix} c_\psi c_\theta & c_\psi s_\theta s_\phi - c_\phi s_\psi & c_\phi c_\psi s_\theta + s_\phi s_\psi \\ c_\theta s_\psi & s_\phi s_\theta s_\psi + c_\phi c_\psi & c_\phi s_\theta s_\psi - s_\phi c_\psi \\ -s_\theta & c_\theta s_\phi & c_\phi c_\theta \end{bmatrix}$$

where ϕ, θ and ψ denote the Euler angles of roll, pitch, and yaw, respectively, with $c_{(*)} = \cos(*)$ and $s_{(*)} = \sin(*)$. In particular, $\boldsymbol{R}(\boldsymbol{\eta})$ is a special orthogonal $SO(3)$ matrix such that $\boldsymbol{R}(\boldsymbol{\eta})^{-1} = \boldsymbol{R}(\boldsymbol{\eta})^T$ and $\det(\boldsymbol{R}(\boldsymbol{\eta})) = 1$, given that $\boldsymbol{R}(\boldsymbol{\eta})$ is invertible.

Consider $\boldsymbol{\eta}$, $\boldsymbol{\xi}$, $\boldsymbol{p}$ and $\boldsymbol{\upsilon}$; the perturbed model of the quadrotor system can be described by the following equations:

$$\dot{\boldsymbol{\eta}} = \boldsymbol{R}_T^{-1}(\boldsymbol{\eta})\,\boldsymbol{\xi} \tag{1a}$$
$$\dot{\boldsymbol{\xi}} = \boldsymbol{f}_1(\boldsymbol{\eta}, \boldsymbol{\xi}) + \Delta \boldsymbol{f}_I(t) + \boldsymbol{J}_P{}^{-1}\tau_\eta \tag{1b}$$
$$\dot{\boldsymbol{p}} = \boldsymbol{\upsilon} \tag{1c}$$
$$\dot{\boldsymbol{\upsilon}} = \boldsymbol{f}_2(\boldsymbol{\upsilon}) - g\boldsymbol{z}_3 + \Delta \boldsymbol{f}_O(t) + \boldsymbol{R}_T(\boldsymbol{\eta})\frac{u_{th}}{m}\boldsymbol{z}_3 \tag{1d}$$
$$\boldsymbol{y} = \boldsymbol{p} \tag{1e}$$

where $\mathbf{X}^T = \left[\boldsymbol{\eta}^T, \boldsymbol{\xi}^T, \boldsymbol{p}^T, \boldsymbol{\upsilon}^T\right] \in \mathbb{R}^{12}$ is the state vector, $\boldsymbol{y}$ is the output vector, $\boldsymbol{J_p} = \text{diag}\left\{J_x, J_y, J_z\right\}$ represents the coefficients of the rotary inertia, $\boldsymbol{\tau_\eta} = \left[\tau_\phi, \tau_\theta, \tau_\psi\right]^T$ denotes the moments in the body-fixed frame, g denotes the acceleration due to gravity, $\boldsymbol{z_3} = [0, 0, 1]^T$, u_{th} denotes the total thrust, m denotes the mass of the quadrotor and $\boldsymbol{R_T}(\boldsymbol{\eta})$ is the matrix relating the rotation angles $\boldsymbol{\eta}$ to the angular velocity $\boldsymbol{\xi}$ and is described as

$$\boldsymbol{R_T}(\boldsymbol{\eta}) = \begin{bmatrix} 1 & 0 & -s_\theta \\ 0 & c_\phi & c_\theta s_\phi \\ 0 & -s_\phi & c_\theta c_\phi \end{bmatrix}, \tag{2}$$

In this model, we assume that $\boldsymbol{f_1} : \mathbb{R}^3 \times \mathbb{R}^3 \to \mathbb{R}^3$ and $\boldsymbol{f_2} : \mathbb{R}^3 \to \mathbb{R}^3$ are sufficiently smooth vector fields on $\mathbf{X}$, which are given by

$$\boldsymbol{f_1}(\boldsymbol{\eta}, \boldsymbol{\xi}) = -\boldsymbol{J_p}^{-1}\left(\boldsymbol{f_g}(\boldsymbol{\xi}) + \boldsymbol{f_a}(\boldsymbol{\eta}, \boldsymbol{\xi}) + \boldsymbol{S}(\boldsymbol{\xi})\boldsymbol{J_p}\boldsymbol{\xi}\right) \tag{3a}$$
$$\boldsymbol{f_2}(\boldsymbol{\upsilon}) = -\frac{1}{m}\boldsymbol{d_p}\boldsymbol{\upsilon} \tag{3b}$$

where $\boldsymbol{d_p} = \text{diag}\left\{d_x, d_y, d_z\right\}$ denotes the air drag coefficients, $\boldsymbol{S}(\boldsymbol{\xi})$ is a skew-symmetric matrix expressed as

$$\boldsymbol{S}(\boldsymbol{\xi}) = \begin{bmatrix} 0 & -r & q \\ r & 0 & -p \\ -q & p & 0 \end{bmatrix}.$$

and $\boldsymbol{f_g}(\boldsymbol{\xi})$ and $\boldsymbol{f_a}(\boldsymbol{\eta}, \boldsymbol{\xi})$ are the gyroscopic effect and aerodynamic friction torques, respectively:

$$\boldsymbol{f_g}(\boldsymbol{\xi}) = \boldsymbol{S}(\boldsymbol{\xi})[i = 1]4\sum(-1)^{i+1}J_i\omega_i\boldsymbol{z_3} \tag{4a}$$
$$\boldsymbol{f_a}(\boldsymbol{\eta}, \boldsymbol{\xi}) = \boldsymbol{d_\eta}\boldsymbol{R_T}^{-1}(\boldsymbol{\eta})\,\boldsymbol{\xi} \tag{4b}$$

where $J_i \in \mathbb{R}$ and $\omega_i \in \mathbb{R}$ denote the moment of inertia and the angular velocity (in rad/sec), respectively, provided by motor i for all $i = \{1, 2, 3, 4\}$ and $\boldsymbol{d_\eta} = \text{diag}\left\{d_\phi, d_\theta, d_\psi\right\}$ denotes the aerodynamic drag coefficients.

The control signal will be constructed in the following section using the thrust u_{th} given by $u_{th} = b\sum_{i=1}^{4}\omega_i^2$ and the torque $\boldsymbol{\tau_\eta}$ given by

$$\boldsymbol{\tau_\eta} = \begin{bmatrix} \tau_\phi \\ \tau_\theta \\ \tau_\psi \end{bmatrix} = \begin{bmatrix} lb\left(\omega_4^2 - \omega_2^2\right) \\ lb\left(\omega_3^2 - \omega_1^2\right) \\ k\left(\omega_2^2 + \omega_4^2 - \omega_1^2 - \omega_3^2\right) \end{bmatrix} \tag{5}$$

where $b\,\omega_i^2$ denotes the lift force provided by motor i; the parameters b and k are positive constants that denote the effects of the drag force, the shape and number of blades and the pitch angle; and l denotes the distance between the motor and the center of gravity.

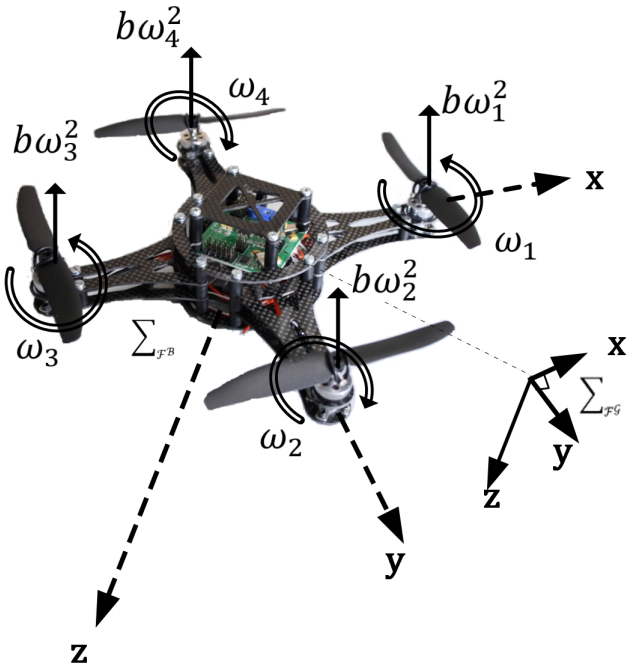

FIGURE 1. The schematic configuration of a quadrotor with the origin of the body-fixed frame and the inertia frame.

Remark 1: In control theory, the robustness of a control system is often defined in relation to disturbances and uncertainties. Thus, robust controllers should be designed to behave ''robustly'' under the estimated matched/unmatched disturbances and uncertainties [33], [39]. In this way, the stability of a closed-loop control system in the presence of the existing disturbances can be guaranteed. To emphasize the novelty of this work, we here discuss the differences between the proposed work and the one published in [18] in terms of the quadrotor modeling. In [18], the authors designed their controllers without considering the estimated uncertainties or disturbances in the model (see Eqs. (1)-(8), (9), and (11) in [18]). Thus, neither the regular sliding mode controller in the inner loop nor the backstepping sliding mode controller in the outer loop was developed to behave robustly in the presence of disturbances or model uncertainties. In this paper, we fill this gap by proposing nonlinear controllers that are developed based on nonlinear control strategies to behave robustly under the estimated internal and external disturbances. Unlike in [18], we incorporate the estimated internal and external disturbances i.e., $\Delta f_I(t)$ and $\Delta f_o(t)$, respectively, in (1), into the quadrotor model. Our controllers are developed to behave robustly under these disturbances.

III. ATTITUDE AND POSITION CONTROLLER DESIGN

In this section, a feedback control system with a two-loop form, i.e. an inner loop and an outer loop, is designed for position trajectory tracking. First, a backstepping sliding mode controller is presented for the inner loop to ensure the trajectory tracking capability of ϕ and θ along the desired roll and pitch angle trajectories ϕ^d, and θ^d, respectively. Next, the outer loop, i.e., the so-called position control subsystem, is designed using robust integral sliding mode control. This controller is mainly designed to overcome the effect of disturbances and generate

1) the desired roll and pitch angle trajectories (ϕ^d, andθ^d), and
2) the thrust control signal (u_{th}).

A. ATTITUDE CONTROL PROBLEM STATEMENT

Consider the perturbed inner-loop subsystem represented by (1a) and (1b), where $\Delta f_I(t) : \mathbb{R} \to \mathbb{R}^3$ denotes the perturbation introduced into the inner-loop system due to noise and discretization. The system is said to be free of perturbation if $\Delta f_I(t) = 0$. The following assumptions are adopted when designing the quadrotor control system.

Assumption 1: The desired reference signals $\boldsymbol{\eta^d}$ and its first and second derivatives, i.e., $\dot{\boldsymbol{\eta}}^{\boldsymbol{d}}$ and $\ddot{\boldsymbol{\eta}}^{\boldsymbol{d}}$, are bounded and available online. Moreover, the disturbance $\Delta f_I(t)$ is bounded such that $\|\Delta f_I(t)\| < \gamma_I$ for some known γ_I.

Assumption 2: In this work, we considered only matched disturbance for ease of analysis.

Our first objective is to develop a robust controller for the attitude control system such that $\boldsymbol{\eta}$ and $\boldsymbol{\xi}$ in (1) track the desired reference signals $\boldsymbol{\eta^d} = \left[\phi^d, \theta^d, \psi^d\right]^T$ and $\boldsymbol{\xi^d} = \left[p^d, q^d, r^d\right]^T$, respectively, in the presence of the perturbation $\Delta f_I(t)$. The tracking errors of the inner-loop control system are as follows:

$$\begin{aligned}\boldsymbol{\eta}^e &= \boldsymbol{\eta^d} - \boldsymbol{\eta}\\ \boldsymbol{\xi}^e &= \boldsymbol{\xi^d} - \boldsymbol{\xi}\\ &= \boldsymbol{R}_T(\boldsymbol{\eta^d})\,\dot{\boldsymbol{\eta}}^d - \boldsymbol{\xi}\end{aligned}$$

where $\boldsymbol{\eta}^d$ can be obtained from the outer loop (to be discussed later) and the desired reference signal $\boldsymbol{\xi^d}$ can be precisely estimated as

$$\boldsymbol{\xi^d} = \boldsymbol{R}_T(\boldsymbol{\eta}^d)\,\dot{\boldsymbol{\eta}}^d \tag{6}$$

using (1a). The change of variables $\boldsymbol{e}_I^T = \left[\boldsymbol{\eta}^{eT} \quad \boldsymbol{\xi}^{eT}\right]$ in (1a) and (1b) yields

$$\dot{\boldsymbol{\eta}}^e = \dot{\boldsymbol{\eta}}^d - \boldsymbol{R}_T^{-1}(\eta)\boldsymbol{\xi^d} + \boldsymbol{R}_T^{-1}(\eta)\boldsymbol{\xi}^e \tag{7a}$$

$$\dot{\boldsymbol{\xi}}^e = \dot{\boldsymbol{\xi}}^d - f_1(\eta, \xi) - \Delta f_I(t) + \boldsymbol{u}_I \tag{7b}$$

where

$$\mathbf{u}_I = -\boldsymbol{J}^{-1}\boldsymbol{\tau}_\eta \tag{8}$$

denotes the attitude controller to be designed. Let

$$\mathbf{u}_I = \mathbf{u}_I^b + \mathbf{u}_I^s \tag{9}$$

where $\mathbf{u}_I^b$ and $\mathbf{u}_I^s$ represent for backstepping and robust sliding mode controllers, respectively.

1) BACKSTEPPING CONTROLLER FOR STABILIZING A PERTURBATION-FREE INNER-LOOP SUBSYSTEM

Let us design a backstepping controller $\mathbf{u}_I^b$ for the case of a perturbation-free inner-loop subsystem by substituting $\Delta \boldsymbol{f}_I(\boldsymbol{t}) = \mathbf{u}_I^s = \mathbf{0}$ into (7) such that

$$\dot{\boldsymbol{\eta}}^e = \dot{\boldsymbol{\eta}}^d - \boldsymbol{R}_T^{-1}(\boldsymbol{\eta})\boldsymbol{\xi}^d + \boldsymbol{R}_T^{-1}(\boldsymbol{\eta})\underline{\boldsymbol{\xi}}^{\mathbf{e}} \tag{10a}$$

$$\dot{\underline{\boldsymbol{\xi}}}^e = \dot{\boldsymbol{\xi}}^d - \boldsymbol{f}_1(\boldsymbol{\eta}, \boldsymbol{\xi}) + \mathbf{u}_I^b \tag{10b}$$

where

$$\dot{\underline{\boldsymbol{\xi}}}^e = \dot{\boldsymbol{\xi}}^e + \Delta \boldsymbol{f}_I(\boldsymbol{t}) - \mathbf{u}_I^s \,. \tag{11}$$

This can be referred to as the nominal inner-loop tracking error.

Clearly, $\underline{\boldsymbol{\xi}}^{\mathbf{e}}$ in (10a) is the virtual input control that can be used to stabilize $\boldsymbol{\eta}^d$. The desired stabilizing function can be selected as follows:

$$\boldsymbol{\Phi} = \boldsymbol{\xi}^d - \boldsymbol{R}_T(\boldsymbol{\eta})\,\boldsymbol{\varrho} \tag{12}$$

where

$$\boldsymbol{\varrho} = \boldsymbol{\Gamma}\boldsymbol{\eta}^e + \dot{\boldsymbol{\eta}}^d \tag{13}$$

in which $\Gamma \in \mathbb{R}^{3\times 3}$ is a designed positive definite matrix.

The stabilizing function given in (12) is selected by replacing $\underline{\boldsymbol{\xi}}^e$ with $\boldsymbol{\Phi}$ in (10a), i.e.,

$$\begin{aligned} 1\dot{\boldsymbol{\eta}}^e &= \dot{\boldsymbol{\eta}}^d - \boldsymbol{R}_T^{-1}(\boldsymbol{\eta})\boldsymbol{\xi}^d + \boldsymbol{R}_T^{-1}(\boldsymbol{\eta})\Big(\boldsymbol{\xi}^d - \boldsymbol{R}_T(\boldsymbol{\eta})\Big)\boldsymbol{\varrho} \\ &= \dot{\boldsymbol{\eta}}^d - \boldsymbol{\varrho} \\ &= -\boldsymbol{\Gamma}\boldsymbol{\eta}^e \end{aligned}$$

which shows that the origin $\boldsymbol{\eta}^e = \mathbf{0}$ is globally exponentially stable. Furthermore, using (6) and (12), it can be shown that

$$\boldsymbol{\Phi}|_{\boldsymbol{\eta}^e=\mathbf{0}} = \boldsymbol{\xi}^d - \boldsymbol{R}_T(\boldsymbol{\eta}^d)\,\dot{\boldsymbol{\eta}}^d = \mathbf{0}. \tag{14}$$

Now let us define a new variable

$$\boldsymbol{\varphi}^e \triangleq \underline{\boldsymbol{\xi}}^e - \boldsymbol{\Phi} \tag{15}$$

and transform (10) into $(\boldsymbol{\eta}^e, \boldsymbol{\varphi}^e)$ coordinates such that

$$\dot{\boldsymbol{\eta}}^e = -\boldsymbol{\eta}^e + \boldsymbol{R}_T^{-1}(\boldsymbol{\eta})\boldsymbol{\varphi}^e \tag{16a}$$

$$\dot{\boldsymbol{\varphi}}^e = \dot{\boldsymbol{\xi}}^d - \boldsymbol{f}_1(\boldsymbol{\eta}, \boldsymbol{\xi}) - \dot{\boldsymbol{\Phi}} + \mathbf{u}_I^b \tag{16b}$$

where

$$\dot{\boldsymbol{\Phi}} = \dot{\boldsymbol{\xi}}^d - \dot{\boldsymbol{R}}_T(\boldsymbol{\eta})\boldsymbol{\varrho} - \boldsymbol{R}_T(\boldsymbol{\eta})\dot{\boldsymbol{\varrho}} \tag{17}$$

with $\dot{\boldsymbol{\varrho}} = \boldsymbol{\Gamma}\dot{\boldsymbol{\eta}}^e + \ddot{\boldsymbol{\eta}}^d$ and

$$\dot{\boldsymbol{R}}_T(\boldsymbol{\eta}) = \begin{bmatrix} 0 & 0 & -\dot{\theta}c_\theta \\ 0 & -\dot{\phi}s_\phi & -\dot{\theta}s_\theta s_\phi + \dot{\phi}c_\theta c_\phi \\ 0 & -\dot{\phi}c_\phi & -\dot{\theta}s_\theta c_\phi - \dot{\phi}c_\theta s_\phi \end{bmatrix}. \tag{18}$$

Taking $V_I^b = \frac{1}{2}\boldsymbol{\eta}^{eT}\boldsymbol{\eta}^e + \frac{1}{2}\boldsymbol{\varphi}^{eT}\boldsymbol{\varphi}^e$ as a composite Lyapunov function (LF), we obtain

$$\begin{aligned} \dot{V} &= \boldsymbol{\eta}^{eT}\dot{\boldsymbol{\eta}}^e + \boldsymbol{\varphi}^{eT}\dot{\boldsymbol{\varphi}}^e \\ &= -\|\boldsymbol{\eta}^e\|^2 + \boldsymbol{\eta}^{eT}\boldsymbol{R}_T^{-1}(\boldsymbol{\eta})\boldsymbol{\varphi}^e + \boldsymbol{\varphi}^{eT}\dot{\boldsymbol{\varphi}}^e \\ &= -\|\boldsymbol{\eta}^e\|^2 + \boldsymbol{\varphi}^{eT}\left(\boldsymbol{R}_T^{-1}(\boldsymbol{\eta})^T\boldsymbol{\eta}^e + \dot{\boldsymbol{\varphi}}^e\right) \end{aligned}$$

Considering (16b) and (17), taking

$$\mathbf{u}_I^b = \dot{\boldsymbol{\Phi}} + \boldsymbol{f}_1(\boldsymbol{\eta}, \boldsymbol{\xi}) - \boldsymbol{R}_T^{-1}(\boldsymbol{\eta})^T\boldsymbol{\eta}^e - \dot{\boldsymbol{\xi}}^d - \boldsymbol{\varphi}^e \tag{19}$$

yields $\dot{V}_I^b = -\left(\|\boldsymbol{\eta}^e\|^2 + \|\boldsymbol{\varphi}^e\|^2\right) < 0$.

Remark 2: This result shows that the origin $\boldsymbol{\eta}^e = \boldsymbol{\varphi}^e = \mathbf{0}$ in (16) is asymptotically stable. Since $\boldsymbol{\varphi}^e = \mathbf{0}$ and $\boldsymbol{\Phi}|_{\boldsymbol{\eta}^e} = \mathbf{0} = \mathbf{0}$ as per (14), we conclude that the origin $\underline{\boldsymbol{\xi}}^e = \mathbf{0}$ is also asymptotically stable.

2) ROBUST SLIDING MODE CONTROLLER FOR AN INNER-LOOP SUBSYSTEM WITH UNCERTAINTY

Given that the desired output should track $\boldsymbol{\eta}^d$ and $\boldsymbol{\xi}^d$, we define the inner-loop sliding surface in the error space as fo1lows:

$$\boldsymbol{s}_I = \begin{bmatrix} \boldsymbol{\eta}^e \\ \boldsymbol{\xi}^e \end{bmatrix} \tag{20}$$

where $\boldsymbol{s}_I \in \mathbb{R}^6$. Clearly, on the sliding surface $\boldsymbol{s}_I = \mathbf{0}$, the trajectory is governed by $\boldsymbol{\eta}^e = \boldsymbol{\xi}^{\mathbf{e}} = \mathbf{0}$. Taking the time derivative of the sliding manifold in (20) yields

$$\dot{\boldsymbol{s}}_I = \begin{bmatrix} \dot{\boldsymbol{\eta}}^e \\ \dot{\boldsymbol{\xi}}^e \end{bmatrix} \tag{21}$$

Consider the LF $V = \frac{1}{2}\boldsymbol{s}_I^T\boldsymbol{s}_I$, which implies that

$$\dot{V} = \boldsymbol{s}_I^T\dot{\boldsymbol{s}}_I \tag{22}$$

Considering the backstepping controller and substituting (21) into (22) yields

$$\dot{V} = \dot{V}(\boldsymbol{\eta}^e, \underline{\boldsymbol{\xi}}^e) + \boldsymbol{\xi}^{eT}\dot{\underline{\boldsymbol{\xi}}}^e \tag{23}$$

where $\dot{V}(\boldsymbol{\eta}^e, \underline{\boldsymbol{\xi}}^e) = \boldsymbol{\eta}^{eT}\dot{\boldsymbol{\eta}}^e + \underline{\boldsymbol{\xi}}^{\mathbf{e}T}\dot{\underline{\boldsymbol{\xi}}}^e$ and $\dot{\underline{\boldsymbol{\xi}}}^e = \mathbf{u}_I^s - \Delta \boldsymbol{f}_I(\boldsymbol{t})$. Given that $\dot{V}(\boldsymbol{\eta}^e, \underline{\boldsymbol{\xi}}^e) \to 0$ as shown in Remark 2, this leads to the following inequality:

$$\dot{V} < -\boldsymbol{\xi}^{eT}\left(\Delta \boldsymbol{f}_I(\boldsymbol{t}) - \boldsymbol{u}_1^s\right) \tag{24}$$

Consider

$$\boldsymbol{u}_I^s = -\beta_I\,\mathbf{Sgn}\left(\boldsymbol{\xi}^e\right) \tag{25}$$

where $\mathbf{Sgn}\left(\boldsymbol{\xi}^e\right) = \left[\operatorname{sgn}(p^e)\ \operatorname{sgn}(q^e)\ \operatorname{sgn}(r^e)\right]^T$ and β_I is the constant to be designed to ensure the robustness of the attitude controller. Substituting (25) into (24) yields

$$\begin{aligned} \dot{V} &< -\boldsymbol{\xi}^{eT}\Delta \boldsymbol{f}_I(\boldsymbol{t}) - \beta_I\left\|\boldsymbol{\xi}^e\right\|_1 \\ &< \left\|\boldsymbol{\xi}^e\right\|\left(\xi_1 - \beta_I\right) \\ &< 0, \qquad \forall\, \beta_I > \xi_1 > 0 \end{aligned} \tag{26}$$

since $\left\|\boldsymbol{\xi}^e\right\|_1 \geq \left\|\boldsymbol{\xi}^e\right\|_p$ for any $p > 1$.

Remark 3: The inner-loop controller (9), consists of two parts: backstepping defined in (19) and sliding mode controller defined in (25). In the first part of the inner-loop controller, we designed backstepping to stabilize the

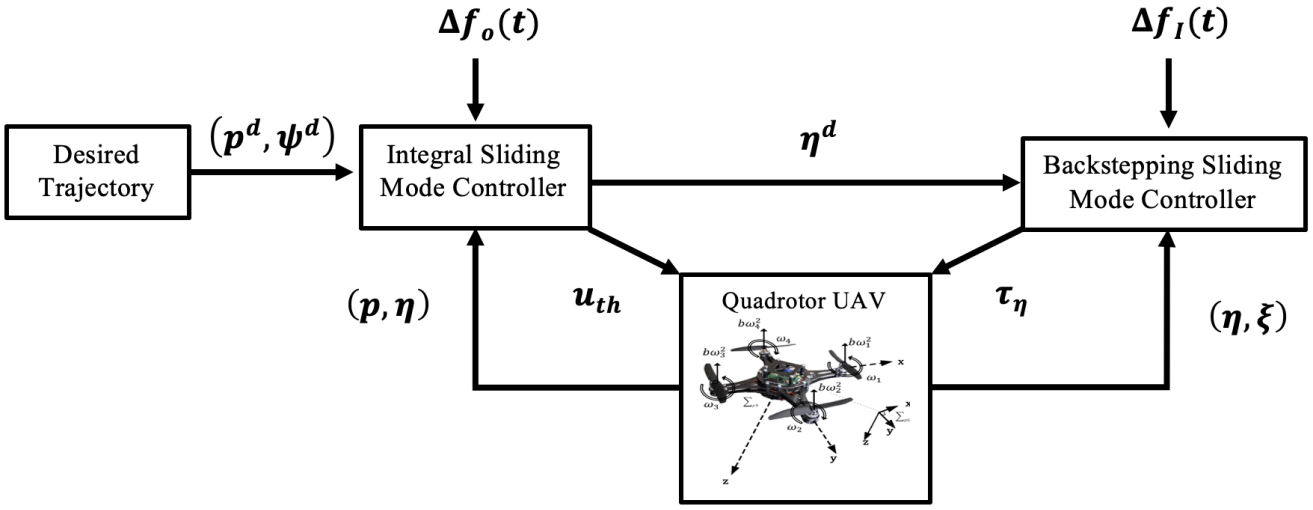

FIGURE 2. Block diagram for the quadrotor control structure.

disturbance-free inner-loop quadrotor sub-system. In the second part, the sliding mode control is designed to work robustly together with backstepping controller against the disturbance. Thus, the proposed inner-loop controller does not have to switch between both backstepping and sliding mode controllers and; therefore, it does not need to have any disturbance detection mechanism.

B. POSITION SUBSYSTEM PROBLEM STATEMENT

Consider the perturbed outer-loop subsystem introduced in (1c) and (1d), where $\boldsymbol{\Delta f_0(t)} : \mathbb{R}^{12} \rightarrow \mathbb{R}^3$ denotes the perturbation introduced into the system due to noise and discretization.

The following assumption is adopted when designing the quadrotor control system.

Assumption 3: The desired output $\boldsymbol{p^d}$ and its first and second derivatives, i.e., $\dot{\boldsymbol{p}} \overset{def}{=} \boldsymbol{v}$ and $\ddot{\boldsymbol{p}}^{\boldsymbol{d}} \overset{def}{=} \dot{\boldsymbol{v}}^{\boldsymbol{d}}$, are bounded and available online. Moreover, the uncertainty $\boldsymbol{\Delta f_0(t)}$ is bounded such that $\left\|\boldsymbol{\Delta f_0(t)}\right\| < \gamma_2$ for some known γ_2.

1) STABILIZING THE OUTER LOOP

The main control objective is to design an outer-loop control system with a robust controller such that $\boldsymbol{p}$ and $\boldsymbol{v}$ in (1c) and (1d) track the desired outputs $\boldsymbol{p^d}$ and $\boldsymbol{v^d}$, respectively. The tracking errors of the outer-loop control system are, therefore, expressed as: $\boldsymbol{p^e} = \boldsymbol{p^d} - \boldsymbol{p}$ and $\boldsymbol{v^e} = \boldsymbol{v^d} - \boldsymbol{v}$.

The change of variables $\boldsymbol{e_o} = \begin{bmatrix} \boldsymbol{p^e} \\ \boldsymbol{v^e} \end{bmatrix}$ in (1c) and (1d) yields

$$\dot{\boldsymbol{p^e}} = \boldsymbol{v^e} \tag{27a}$$
$$\dot{\boldsymbol{v}}^{\boldsymbol{e}} = \ddot{\boldsymbol{p}}^{\boldsymbol{d}} - \dot{\boldsymbol{v}}^{\boldsymbol{e}} \tag{27b}$$

If we assume that the desired ψ^d, that is the desired yaw (ψ), is provided along with the waypoints, then we have the remaining desired inputs, i.e., the roll ϕ^d, the pitch θ^d, and the total torque u_T, to reconstruct the control. Let

$$\boldsymbol{u_o} = \text{col}\left(\phi^d,\ \theta^d,\ u_T\right) \tag{28}$$

denote the robust control inputs for perturbed outer loop that is to be designed.

Let us define the outer-loop sliding-surface function as follows:

$$\boldsymbol{s_o} = \alpha_1 \int_{-\infty}^{t} \boldsymbol{p^e} d\tau + \alpha_2 \boldsymbol{p^e} + \dot{\boldsymbol{p}}^{\boldsymbol{e}} \tag{29}$$

where α_1 and α_2 are selected to be positive constants. Taking time derivative of the sliding manifold in (29) and using (27b) yields

$$\dot{\mathbf{s}}_o = \alpha_1 \boldsymbol{p^e} + \alpha_2 \dot{\boldsymbol{p}}^{\boldsymbol{e}} + \ddot{\boldsymbol{p}}^{\boldsymbol{e}} \tag{30a}$$
$$= \alpha_1 \boldsymbol{p^e} + \alpha_2 \boldsymbol{v^e} + \dot{\boldsymbol{v}}^{\boldsymbol{e}} \tag{30b}$$
$$= \mathbf{E}\,(\boldsymbol{p},\, \boldsymbol{v}) - \boldsymbol{\Delta f_o(t)} - \boldsymbol{R(\eta)} z_3 u_T \tag{30c}$$

where $u_T = \frac{u_{th}}{m}$ and

$$\mathbf{E}\,(\boldsymbol{p},\, \boldsymbol{v}) = \alpha_1 \boldsymbol{p^e} + \alpha_2 \boldsymbol{v^e} + \ddot{\boldsymbol{p}}^{\boldsymbol{d}} + g z_3 - \boldsymbol{f_2}(\boldsymbol{v}) \tag{31}$$

For the equivalent sliding mode control, where $\boldsymbol{s_o} \dot{=} 0$, and given that α_1 and α_2 are positive definite matrices, it is easy to show that (30a) satisfies the following Hurwitz polynomial: $\lambda^2 + \alpha_2 \lambda + \alpha_1 = 0$. Therefore, the position error will converge to zero under the appropriate control design.

Let

$$\boldsymbol{R(\eta)} z_3 u_T = \hat{\mathbf{E}}(\boldsymbol{p},\, \boldsymbol{v}) \tag{32}$$

with $\hat{\mathbf{E}}(\boldsymbol{p},\, \boldsymbol{v})$ defined as

$$\hat{\mathbf{E}}(\boldsymbol{p},\, \boldsymbol{v}) \triangleq \begin{bmatrix} \varepsilon_1 \\ \varepsilon_2 \\ \varepsilon_3 \end{bmatrix} = \mathbf{E}\,(\boldsymbol{p},\, \boldsymbol{v}) + \beta_o\, \mathbf{Sgn}\,(\mathbf{s_o}) \tag{33}$$

where β_o is the constant to be designed to ensure robustness in the outer loop. Assume that the desired yaw (ψ^d in assumption 1) is provided along with the waypoints. Under this

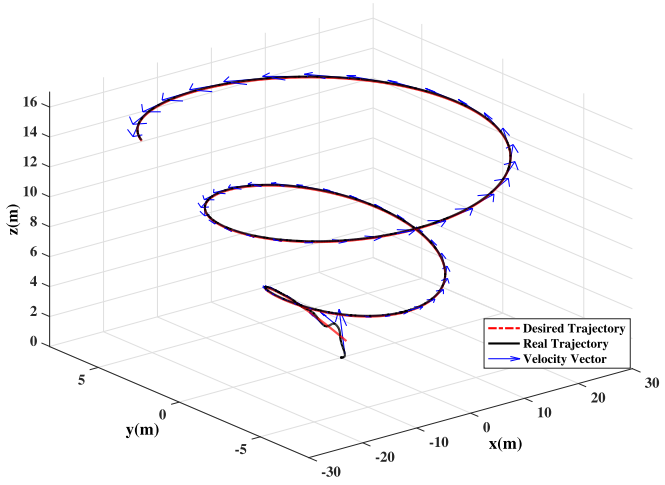

(a) Three-dimensional trajectory tracking perturbation-free control system

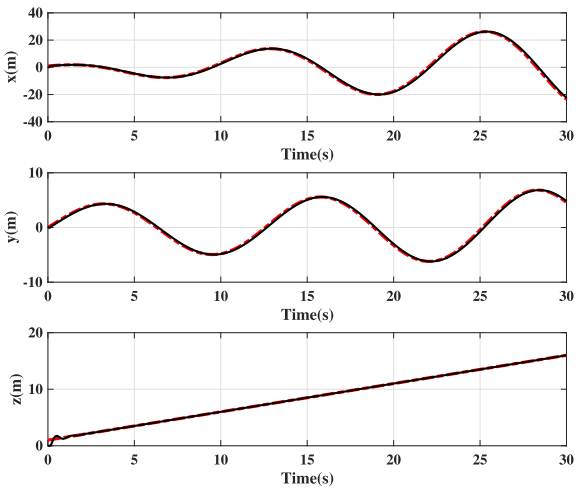

(b) Desired position response $(p^d)$and actual position response (p)

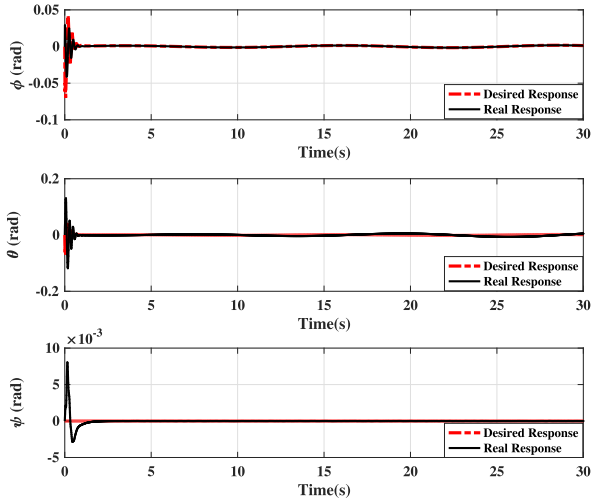

(c) Desired Euler's angle response (η^d) and actual Euler angles response (η)

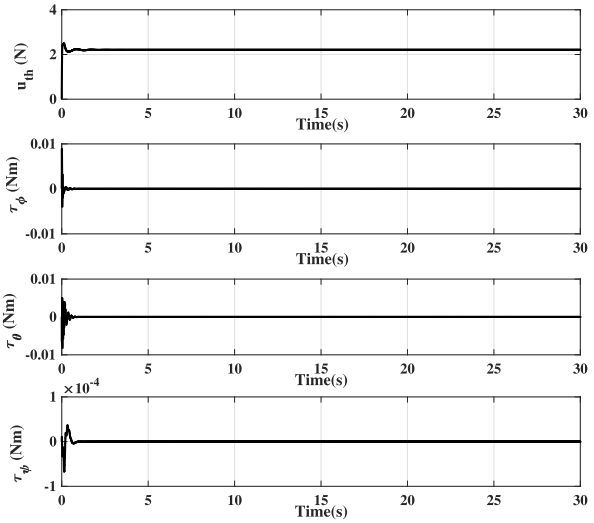

(d) The virtual control inputs: total thrust (τ_T) and rotational torques $(\tau_{\phi,\theta,\psi})$

FIGURE 3. The performance of the tracking trajectory for perturbation-free control systems.

assumption, (32) basically consists of three equations with three manipulated inputs, i.e., the desired roll ϕ^d, the desired pitch θ^d, and u_T, which can be found by solving (32). After simple algebraic computations, the following equations are obtained:

$$\phi^d = \arcsin\left(\frac{\varepsilon_1 s_{\psi^d} - \varepsilon_2 c_{\psi^d}}{\left\|\hat{\mathbf{E}}(\boldsymbol{p},\boldsymbol{v})\right\|_2}\right) \tag{34a}$$

$$\theta^d = \arctan\left(\frac{\varepsilon_1 c_{\psi^d} + \varepsilon_2 s_{\psi^d}}{\varepsilon_3}\right) \tag{34b}$$

Substituting (34) into (32) yields $z_3 u_T = \boldsymbol{R}(\boldsymbol{\eta^d})^T \hat{\boldsymbol{E}}(\boldsymbol{p},\boldsymbol{v})$ since $\boldsymbol{R}(\boldsymbol{\eta^d})^{-1} = \boldsymbol{R}(\boldsymbol{\eta^d})^T$. Equivalently,

$$u_T = \begin{bmatrix} c_{\phi^d} c_{\psi^d} s_{\theta^d} + s_{\psi^d} s_{\phi^d} \\ s_{\theta^d} s_{\psi^d} c_{\phi^d} - c_{\psi^d} s_{\phi^d} \\ c_{\phi^d} c_{\theta^d} \end{bmatrix}^T \hat{\mathbf{E}}(\boldsymbol{p},\boldsymbol{v}). \tag{35}$$

If β_o is selected such that

$$\beta_o \geq \gamma_2 > \left\|\Delta \boldsymbol{f}_o(\boldsymbol{t})\right\| \tag{36}$$

then it is easy then to show that $\boldsymbol{s}_o^T \dot{\boldsymbol{s}}_o < 0$ holds.

Remark 4: To emphasize the novelty of this work, we here present the major differences between our work and the one published in [18] in terms of control structure. The work [18] proposed a backstepping sliding mode control technique for the outer loop to achieve position trajectory tracking for a quadrotor. They first developed a regular sliding mode controller for the attitude subsystem (inner loop) to guarantee fast convergence of the Euler angles. Then, the backstepping sliding mode control technique was applied for position control (outer loop) to generate the desired attitude (Euler angles). By contrast, in our work, we develop a robust backstepping sliding mode controller for the inner loop and a robust integral sliding mode controller for the outer loop.

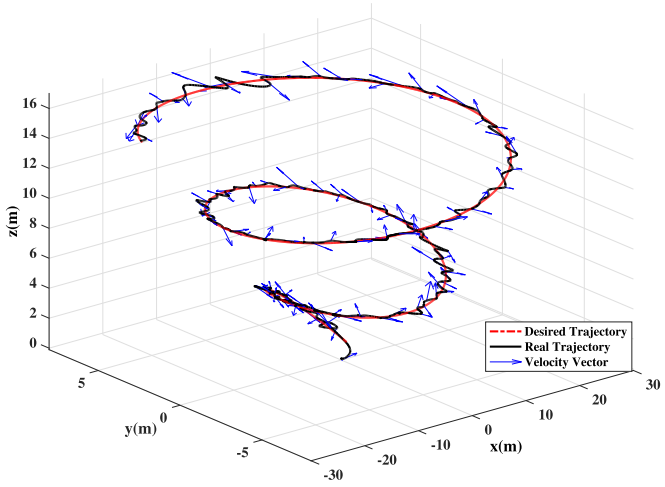

(a) Three-dimensional trajectory tracking for the perturbed control system

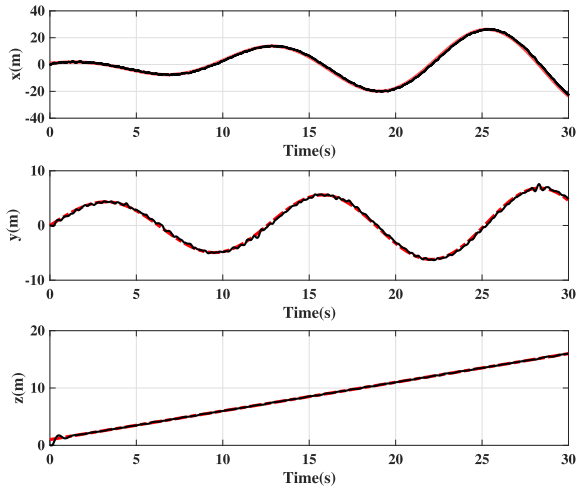

(b) Desired position response p^d and actual position response p

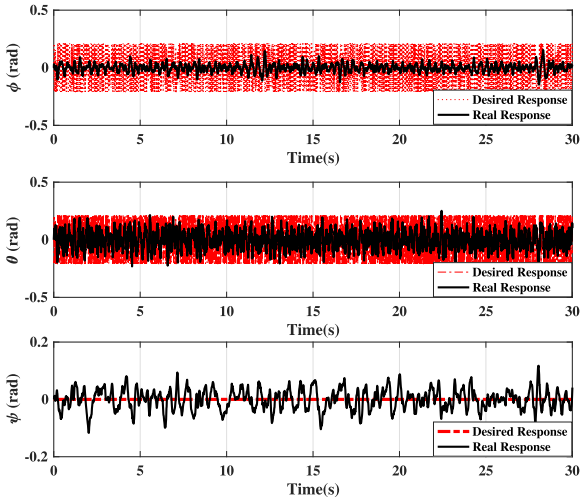

(c) Desired Euler's angle response (η^d) and actual Euler's angles response (η)

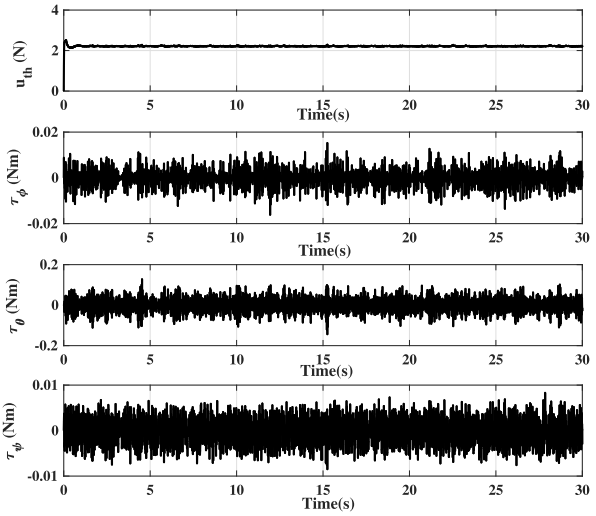

(d) The virtual control inputs: total thrust (τ_T) and rotational torques $(\tau_{\phi,\theta,\psi})$

FIGURE 4. The performance of the tracking trajectory for the perturbed control system.

Remark 5: In future work, it may be of interest to consider replacing (29) with the recent integral or adaptive sliding mode laws augmented with neural network proposed in [40]–[45].

IV. SIMULATION

Here, the performance of the proposed control strategy is illustrated through extensive numerical simulations using MATLAB/Simulink. In this study, we consider the quadrotor model given in (1)-(5) with the identified parameters given in Table 1 and *zero* initial conditions for all states, i.e. $\boldsymbol{\eta} = \boldsymbol{\xi} = \boldsymbol{p} = \boldsymbol{v} = \mathbf{0}$.

A. SIMULATION RESULTS

The two controllers, i.e., the inner-loop backstepping-based sliding mode controller defined in (9), (19) and (25) and the outer-loop integral sliding mode defined in (28), (34) and (35), are applied to validate the robustness and trajectory tracking performance of the proposed scheme. The desired trajectory is chosen to be

$$\boldsymbol{p^d} = \begin{bmatrix} (1+t)\,cos(0.5t) \\ (4+0.1t)\,sin(0.5t) \\ 1+0.5t \end{bmatrix}$$

and the desired yaw is initially set to *zero*, i.e., $\psi^d = 0$. It is obvious that $\boldsymbol{p^d} = [1, 0, 1]$ at $t = 0$. Thus, the mission of the

TABLE 1. Quadrotor model parameters.

Symbol	Value	Symbol	Value
m	$0.47\ kg$	$J_{x,y}$	$4.9 \times 10^{-3}\ \ kg\,m^2$
g	$9.81\ m/s^2$	J_z	$8.8 \times 10^{-3}\ \ kg\,m^2$
l	$0.225\ m$	b	$2.9 \times 10^{-6}\ Ns^2/rad^2$
$J_{1,\ldots,4}$	$3.4 \times 10^{-5}\ kg\,m^2$	k	$1.14 \times 10^{-7}\ Ns^2/rad^2$
$d_{x,y,z}$	4.001×10^{-7}	$d_{\phi,\theta,\psi}$	6.01×10^{-5}

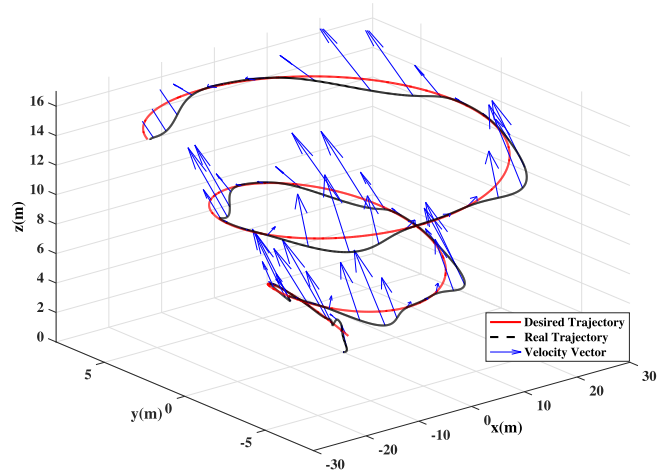

(a) Three-dimensional quadrotor trajectory tracking with wind disturbances

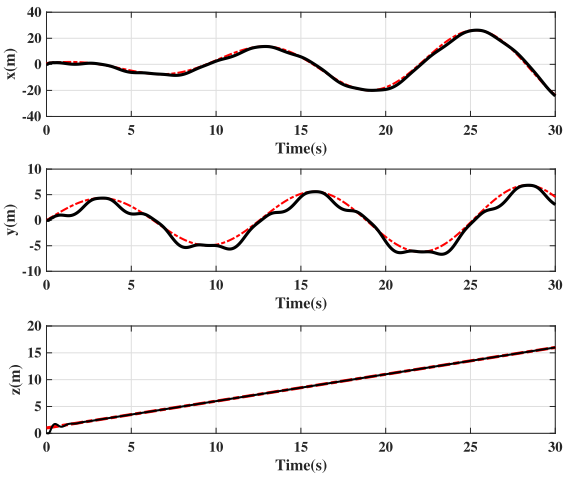

(b) Desired position response p^d and actual position response p

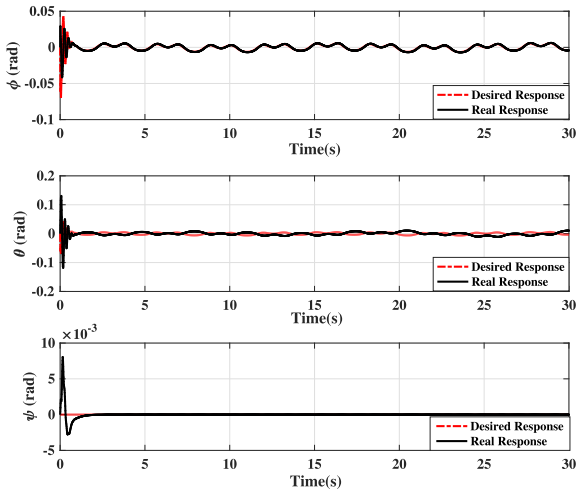

(c) Desired Euler's angle response (η^d) and actual Euler's angles response (η)

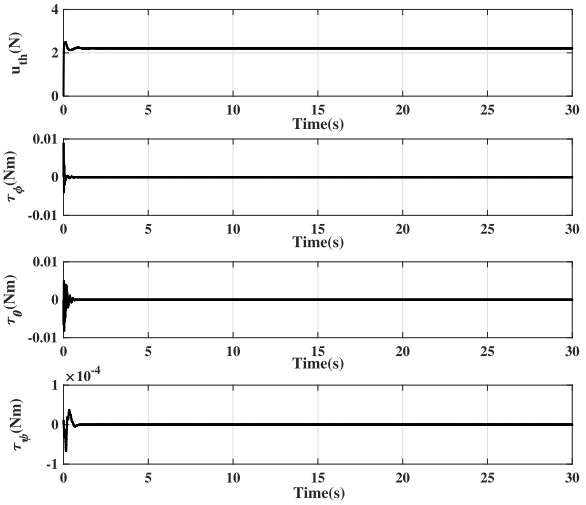

(d) The virtual control inputs: total thrust (u_{th}) and rotational torques $(\tau_{\phi,\theta,\psi})$

FIGURE 5. The performance of the tracking trajectory for the quadrotor control system with wind disturbances.

quadrotor is to start from the origin [0, 0, 0] and to proceed to [1, 0, 1].

To explore the effectiveness of our proposed controller, the following three scenarios are considered. Each simulation lasts for 30 seconds.

Scenario I: In this scenario, numerical simulations are carried out for the perturbation-free case (trajectory tracking with the designed parameters given in Table 2). As shown in the table, the parameters of the robust controllers, i.e., β_I in (25) and β_o in (33), are designed to be small as possible. The performance of the proposed tracking control strategy is illustrated in Fig. 3. The three-dimensional path (see Fig. 3.(a)) shows that when the proposed scheme is applied, the quadrotor successfully achieves the desired waypoint tracking with very low control effort (see Fig. 3.(d)). It is obvious that the velocity vector is directed toward the desired path. Fig. 3.(a) and (b) demonstrate that the transition time

TABLE 2. Controller parameters.

Controller	Case I	Case II	Case III
Parameter	$\Delta f_I = 0$ $\Delta f_o = 0$ $\psi^d = 0$	$\|\Delta f_I\|_\infty = 1$ $\|\Delta f_o\|_\infty = 1$ $\psi^d = 0$	$\|\Delta f_I\|_\infty = 1$ $\|\Delta f_o\|_\infty = 2$ $\psi^d = 0$
$\Gamma(13)$	$5.0\, I_3$	$5.0\, I_3$	$5.0\, I_3$
$\beta_I(25)$	0.01	1.0	1.0
$\alpha_{1,2}(29)$	5.0	5.0	5.0
$\beta_o(33)$	0.01	1.5	2.0

required to move from the origin [0, 0, 0] to [1, 0, 1] is less than *one* second, with less that 10% overshoot (see z^d and z in Fig. 3.(b) and the thrust u_{th} in Fig. 3.(d)).

Scenario II: In this scenario, we consider trajectory tracking with uncertainty with the designed parameters given in Table 2. The perturbation comes from high-frequency additive white Gaussian noise ($\|\Delta f_I\|_\infty = \|\Delta f_o\|_\infty = 1$), which is added to the feedback signals from the noisy

communication channels that connect the ground station to the onboard processor or is generated by the undesirable weather conditions (e.g., external wind gusts) and directly affects the center of mass of the body.

As shown in Table 2, the robust property of the proposed scheme is activated when the parameters, β_I in (25) and β_o in (33), are designed to satisfy the stability conditions given in (26) and (36), respectively. The performance of the proposed tracking control strategy is depicted in Fig. 4. The three-dimensional path in Fig. 4.(a) and the actual position response in Fig. 4.(b) show that the proposed scheme succeeds in tracking the desired tracking with a very small tracking error and little deviation to the left and right in the X-Y plane.

Scenario III: In this scenario, we consider trajectory tracking with wind disturbances. The designed parameters of the proposed controllers are given in Table 2. The perturbation comes from wind gust with varying wind speed less than $2\,m/s$, that is directly applied to the v^x, v^y and v^z-axises. The considered wind guest in this scenario results in $\|\Delta f_I\|_\infty = 1$ and $\|\Delta f_o\|_\infty = 2$.

As shown in Table 2, the parameters β_I in (25) and β_o in (33), are designed to satisfy the stability conditions given in (26) and (36), respectively. The performance of the proposed tracking control strategy is depicted in Fig. 5. The three-dimensional path in Fig. 5.(a) shows that the proposed scheme succeeds in tracking the desired tracking with a small tracking error and little deviation to the left and right in the X-Y plane. The peak position errors in the steady state are $\boldsymbol{p^e} \approx [0.5, 1.9, 0.05]^T$ as shown in Fig. 5.(b).

V. CONCLUSION

In this paper, robust nonlinear control strategies for a quadrotor subject to uncertainties have been presented. The proposed control algorithm, which combines integral sliding mode and backstepping sliding mode controllers in a double-loop control structure, effectively ensures the trajectory tracking capability for the desired position. The stability and performance of the quadrotor control system has been thoroughly investigated through Lyapunov stability analysis. Numerical simulations demonstrate the effectiveness of the developed solutions for a quadrotor. The simulation results demonstrate that the proposed control algorithm effectively controls the quadrotor system and achieves the desired specifications even under sever uncertainties.

REFERENCES

[1] P. Ross, J. Romero, W. Jones, A. Bleicher, J. Calamia, J. Middleton, R. Stevenson, S. Moore, S. Upson, D. Schneider, W. Jones, E. Guizzo, T. Perry, and G. Zorpette, "Top 11 technologies of the decade," *IEEE Spectr.*, vol. 48, no. 1, pp. 27–63, Jan. 2011.
[2] S. Bouabdallah, A. Noth, and R. Siegwart, "PID vs LQ control techniques applied to an indoor micro quadrotor," in *Proc. IEEE/RSJ Int. Conf. Intell. Robots Syst. (IROS)*, vol. 3, Sep. 2004, pp. 2451–2456.
[3] P. E. I. Pounds, D. R. Bersak, and A. M. Dollar, "Stability of small-scale UAV helicopters and quadrotors with added payload mass under PID control," *Auton Robot*, vol. 33, nos. 1–2, pp. 129–142, Aug. 2012.
[4] S. Grzonka, G. Grisetti, and W. Burgard, "A fully autonomous indoor quadrotor," *IEEE Trans. Robot.*, vol. 28, no. 1, pp. 90–100, Feb. 2012.
[5] V. Ghadiok, J. Goldin, and W. Ren, "On the design and development of attitude stabilization, vision-based navigation, and aerial gripping for a low-cost quadrotor," *Auton Robot*, vol. 33, nos. 1–2, pp. 41–68, Aug. 2012.
[6] B. Erginer and E. Altug, "Modeling and PD control of a quadrotor VTOL vehicle," in *Proc. IEEE Intell. Vehicles Symp.*, Jun. 2007, pp. 894–899.
[7] A. Tayebi and S. Mcgilvray, "Attitude stabilization of a VTOL quadrotor aircraft," *IEEE Trans. Contr. Syst. Technol.*, vol. 14, no. 3, pp. 562–571, May 2006.
[8] H. Liu, G. Lu, and Y. Zhong, "Robust LQR attitude control of a 3-DOF laboratory helicopter for aggressive maneuvers," *IEEE Trans. Ind. Electron.*, vol. 60, no. 10, pp. 4627–4636, Oct. 2013.
[9] T. J. Koo and S. Sastry, "Output tracking control design of a helicopter model based on approximate linearization," in *Proc. 37th IEEE Conf. Decis. Control*, vol. 4, Dec. 1998, pp. 3635–3640.
[10] A. Isidori, L. Marconi, and A. Serrani, "Robust nonlinear motion control of a helicopter," *IEEE Trans. Autom. Control*, vol. 48, no. 3, pp. 413–426, Mar. 2003.
[11] V. Gavrilets, *Dynamic Model for a Miniature Aerobatic Helicopter*. Dordrecht, The Netherlands: Springer, 2015, pp. 279–306.
[12] E. Altug, J. P. Ostrowski, and R. Mahony, "Control of a quadrotor helicopter using visual feedback," in *Proc. IEEE Int. Conf. Robot. Autom.*, vol. 1, May 2002, pp. 72–77.
[13] V. Mistler, A. Benallegue, and N. K. M'Sirdi, "Exact linearization and noninteracting control of a 4 rotors helicopter via dynamic feedback," in *Proc. 10th IEEE Int. Workshop Robot Hum. Interact. Commun. (ROMAN)*, Sep. 2001, pp. 586–593.
[14] A. Mokhtari, N. K. M'sirdi, K. Meghriche, and A. Belaidi, "Feedback linearization and linear observer for a quadrotor unmanned aerial vehicle," *Adv. Robot.*, vol. 20, no. 1, pp. 71–91, Jan. 2006.
[15] D. Lee, H. Jin Kim, and S. Sastry, "Feedback linearization vs. Adaptive sliding mode control for a quadrotor helicopter," *Int. J. Control Autom. Syst.*, vol. 7, no. 3, pp. 419–428, Jun. 2009.
[16] A. Das, F. Lewis, and K. Subbarao, "Dynamic inversion with zero-dynamics stabilisation for quadrotor control," *IET Control Theory Appl.*, vol. 3, no. 3, pp. 303–314, Mar. 2009.
[17] S. Bertrand, N. Guénard, T. Hamel, H. Piet-Lahanier, and L. Eck, "A hierarchical controller for miniature VTOL UAVs: Design and stability analysis using singular perturbation theory," *Control Eng. Pract.*, vol. 19, no. 10, pp. 1099–1108, Oct. 2011.
[18] F. Chen, R. Jiang, K. Zhang, B. Jiang, and G. Tao, "Robust backstepping sliding-mode control and observer-based fault estimation for a quadrotor UAV," *IEEE Trans. Ind. Electron.*, vol. 63, no. 8, pp. 5044–5056, Aug. 2016.
[19] I. González, S. Salazar, and R. Lozano, "Chattering-free sliding mode altitude control for a quad-rotor aircraft: Real-time application," *J. Intell. Robotic Syst.*, vol. 73, pp. 137–155, Jan. 2014.
[20] I. Gonzalez-Hernandez, S. Salazar, R. Lopez, and R. Lozano, "Altitude control improvement for a quadrotor UAV using integral action in a sliding-mode controller," in *Proc. Int. Conf. Unmanned Aircraft Syst. (ICUAS)*, pp. 711–716, Jun. 2016.
[21] B. Mu, K. Zhang, and Y. Shi, "Integral sliding mode flight controller design for a quadrotor and the application in a heterogeneous multi-agent system," *IEEE Trans. Ind. Electron.*, vol. 64, no. 12, pp. 9389–9398, Dec. 2017.
[22] T. Madani and A. Benallegue, "Backstepping control for a quadrotor helicopter," in *Proc. IEEE/RSJ Int. Conf. Intell. Robots Syst.*, Oct. 2006, pp. 3255–3260.
[23] Z. Zuo, "Trajectory tracking control design with command-filtered compensation for a quadrotor," *IET Control Theory Appl.*, vol. 4, no. 11, pp. 2343–2355, Nov. 2010.
[24] S. Bouabdallah and R. Siegwart, "Full control of a quadrotor," in *Proc. IEEE/RSJ Int. Conf. Intell. Robots Syst.*, Oct. 2007, pp. 153–158.
[25] O. Garcia, P. Ordaz, O. Santos-Sanchez, S. Salazar, and R. Lozano, "Backstepping and robust control for a quadrotor in outdoors environments: An experimental approach," *IEEE Access*, vol. 7, pp. 40636–40648, 2019.
[26] N. Fethalla, M. Saad, H. Michalska, and J. Ghommam, "Robust observer-based dynamic sliding mode controller for a quadrotor UAV," *IEEE Access*, vol. 6, pp. 45846–45859, 2018.
[27] B. Zhao, Y. Tang, C. Wu, and W. Du, "Vision-based tracking control of quadrotor with backstepping sliding mode control," *IEEE Access*, vol. 6, pp. 72439–72448, 2018.
[28] Z. Zuo and S. Mallikarjunan, "$\mathcal{L}_1$ adaptive backstepping for robust trajectory tracking of UAVs," *IEEE Trans. Ind. Electron.*, vol. 64, no. 4, pp. 2944–2954, Apr. 2017.

[29] T. Lee, "Robust adaptive attitude tracking on *SO*(3) with an application to a quadrotor UAV," *IEEE Trans. Contr. Syst. Technol.*, vol. 21, no. 5, pp. 1924–1930, Sep. 2013.
[30] B. Zhao, B. Xian, Y. Zhang, and X. Zhang, "Nonlinear robust adaptive tracking control of a quadrotor UAV via immersion and invariance methodology," *IEEE Trans. Ind. Electron.*, vol. 62, no. 5, pp. 2891–2902, May 2015.
[31] R. C. Avram, X. Zhang, and J. Muse, "Nonlinear adaptive fault–tolerant quadrotor altitude and attitude tracking with multiple actuator faults," *IEEE Trans. Contr. Syst. Technol.*, vol. 26, no. 2, pp. 701–707, Mar. 2018.
[32] S. Mallavalli and A. Fekih, "A fault tolerant control design for actuator fault mitigation in quadrotor UAVs," in *Proc. Amer. Control Conf. (ACC)*, Jul. 2019, pp. 5111–5116.
[33] H. K. Khalil, *Nonlinear System*, 3rd ed. Upper Saddle River, NJ, USA: Prentice-Hall, 2002.
[34] B. Mu, Y. Pei, and Y. Shi, "Integral sliding mode control for a quadrotor in the presence of model uncertainties and external disturbances," in *Proc. Amer. Control Conf. (ACC)*, May 2017, pp. 5818–5823.
[35] J.-J. Xiong and E.-H. Zheng, "Position and attitude tracking control for a quadrotor UAV," *ISA Trans.*, vol. 53, no. 3, pp. 725–731, 2014.
[36] A. Das, F. Lewis, and K. Subbarao, "Backstepping approach for controlling a quadrotor using Lagrange form dynamics," *J. Intell. Robotic Syst.*, vol. 56, pp. 127–151, Sep. 2009.
[37] G. V. Raffo, M. G. Ortega, and F. R. Rubio, "Robust nonlinear control for path tracking of a quad–rotor helicopter," *Asian J. Control*, vol. 17, no. 1, pp. 142–156, Jan. 2015.
[38] M. E. Antonio-Toledo, E. N. Sanchez, A. Y. Alanis, J. Flórez, and M. A. Perez-Cisneros, "Real–time integral backstepping with sliding mode control for a quadrotor UAV," *IFAC-PapersOnLine*, vol. 51, no. 13, pp. 549–554, 2018.
[39] V. I. Utkin, *Sliding Modes in Control and Optimization*. Berlin, Germany: Springer, 1992.
[40] J. Sun, Y. Shen, X. Wang, and J. Chen, "Finite-time combination-combination synchronization of four different chaotic systems with unknown parameters via sliding mode control," *Nonlinear Dyn.*, vol. 76, no. 1, pp. 383–397, Apr. 2014.
[41] J. Sun, Y. Wang, Y. Wang, and Y. Shen, "Finite-time synchronization between two complex-variable chaotic systems with unknown parameters via nonsingular terminal sliding mode control," *Nonlinear Dyn.*, vol. 85, no. 2, pp. 1105–1117, Jul. 2016.
[42] J. Sun, Y. Wu, G. Cui, and Y. Wang, "Finite-time real combination synchronization of three complex-variable chaotic systems with unknown parameters via sliding mode control," *Nonlinear Dyn.*, vol. 88, no. 3, pp. 1677–1690, May 2017.
[43] J. Sun, X. Zhao, J. Fang, and Y. Wang, "Autonomous memristor chaotic systems of infinite chaotic attractors and circuitry realization," *Nonlinear Dyn.*, vol. 94, no. 4, pp. 2879–2887, Dec. 2018.
[44] Y. Chu, J. Fei, and S. Hou, "Adaptive global sliding-mode control for dynamic systems using double hidden layer recurrent neural network structure," *IEEE Trans. Neural Netw. Learn. Syst.*, to be published.
[45] J. Sun, G. Han, Z. Zeng, and Y. Wang, "A memristor-based neural network circuit of full-function pavlov associative memory with time delay and variable learning rate," *IEEE Trans. Cybern.*, to be published.

DHAFER J. ALMAKHLES (Member, IEEE) received the B.E. degree in electrical engineering from the King Fahd University of Petroleum and Minerals, Dhahran, Saudi Arabia, in 2006, and the master's degree (Hons.) and the Ph.D. degree from The University of Auckland, New Zealand, in 2011 and 2016, respectively. Since 2016, he has been with Prince Sultan University, Saudi Arabia, where he is currently the Chairman of the Communications and Networks Engineering Department, and the Director of the Science and Technology Unit and Intellectual Property Office, Prince Sultan University. He is the leader of the Renewable Energy Research Team and Laboratory. His research interests include control theory, signal processing, unmanned aerial vehicles, renewable energy systems, and FPGA applications. He is a member of the IEEE Power Electronics and the IEEE Control Society. He is a Reviewer Member of various international journals and conferences, including the IEEE and IET.